Optics Communications 284 (2011) 4022–4027

Contents lists available at ScienceDirect

Optics Communications

journal homepage: www.elsevier.com/locate/optcom

Reflection chromaticity of cholesteric liquid crystals with sandwiched periodical isotropic defect layers

Zhenghong He [a,b], Zhicheng Ye [a,*], Qingyu Cui [a], Jiliang Zhu [a], Hongyue Gao [a], Yuye Ling [a], Hongqing Cui [c], Jiangang Lu [a], Xiaojun Guo [a], Yikai Su [a]

[a] SEIEE, Display & Lighting Center, Shanghai Jiao Tong University, National Engineering Lab of TFT-LCD Materials and Technologies, Shanghai, 200240, China
[b] School of Physical Science and Technology, Southwest University, Chongqing, 400715, China
[c] LCD R&D Center, Infovision Optoelectronics Crop., Jiangsu, China

ARTICLE INFO

Article history:
Received 10 September 2010
Received in revised form 1 April 2011
Accepted 5 April 2011
Available online 28 April 2011

Keywords:
Cholesteric liquid crystals
Defect
Photonic crystals
Chromaticity

ABSTRACT

We study one-dimensional photonic crystals made of cholesteric liquid crystals with sandwiched isotropic defect layers. Based on the Berreman Fast 4×4 matrix method, the dispersion relation of one-dimensional photonic crystals is calculated and the corresponding reflection chromaticity is obtained. It is found that the color shift could be controlled by adjusting the thickness and refractive index of the isotropic defect layers. Compared with conventional structures, the reflection chromaticity of this structure is insensitive to the incident angle, if the thickness ratio of the cholesteric liquid crystals to that of the isotropic defect layers and the refractive index of periodical isotropic defect layers are properly set. Furthermore, the common forbidden bands for both left and right circular polarizations can be obtained, and we also take the wavelength-dependent refractive indices into consideration and obtain the reflected light chromaticity with the incident angle increasing. The proposed device can be used as a reflective color filter in the display industry.

1. Introduction

Photonic crystals (PCs) are artificial structures with periodic permittivity [1,2], which have photonic band gaps (PBGs). The propagation of light with wavelengths within the PBGs is prohibited. With these inherent characteristics, PCs have attracted wide attention in many applications, such as optical switches [3,4], tunable filters [5–7], waveguides [8], and etc. [9,10]. Recently, research interest has been extended to PCs made of cholesteric liquid crystals (ChLCs), due to the inherent periodic helical order, i.e. natural one-dimensional PCs. In ChLCs, the PBGs depend on the birefringence and the pitch of the LC helical structure and can be conveniently tuned as active devices.

The defects of the PCs can be introduced by replacing a part of the host medium with a material of different dielectric constant. In this case, defect modes can appear in the PBGs. Based on this principle, some types of defects in ChLCs have been investigated. Schmidtke and Kopp et al. studied a defect caused by the jump of helix phase on the boundary of two ChLCs layers [11–13]; Yang et al. demonstrated a thin layer of isotropic substance between two ChLCs layers [14]; Matsui et al. showed a defect caused by changing the helix pitch locally [15], and several other structures without periodic defects using single-pitched ChLCs have also been investigated. Those structures demonstrated a single reflection color for electromagnetic waves with the same chirality of the LCs.

In this paper, we investigate the photonic properties of one-dimensional PCs made of ChLC with sandwiched periodic isotropic defect layers (IDLs) [16–18]. Using the Berreman Fast 4×4 matrix method, the optical Eigen modes and the reflection spectra are calculated, and then the chromaticity diagrams are obtained according to the International Commission on Illumination (CIE). Our results demonstrated two color reflection bands in the visible region with little dependence on the incident angle. Moreover, the left and right circularly polarized lights have common reflection bands, and the ChLC-IDLs system provides new opportunities in photonic applications such as wide-band color filters, reflectors, polarizers, microcavities for organic lasers or light-emitting diodes and reflective displays [17].

In the simulations, we consider a plane wave incident to the surface of a ChLC-IDLs device with an oblique angle, as shown in Fig. 1. Without losing the generality, the *xyz* coordinate system can be properly selected to ensure that the incident wave vector **k** lies on the *x–z* plane which is parallel to the surface of ChLC-IDLs, while the +x axis is perpendicular to the surface of ChLC-IDLs.

In the periodic structures, ChLCs are distributed in the structures except the regions where the IDLs are introduced. The handedness of the host ChLCs is assumed to be right along the x direction. The pitch of the ChLCs p is 0.345 μm, and the refractive index of the surrounding of the structure {n_{0}} is 1.5. The extraordinary refractive index of LCs $n_e = 1.7$, the ordinary refractive index $n_o = 1.5$, and the thickness

* Corresponding author.
E-mail address: yzhch@sjtu.edu.cn (Z. Ye).

0030-4018/$ – see front matter © 2011 Elsevier B.V. All rights reserved.
doi:10.1016/j.optcom.2011.04.015

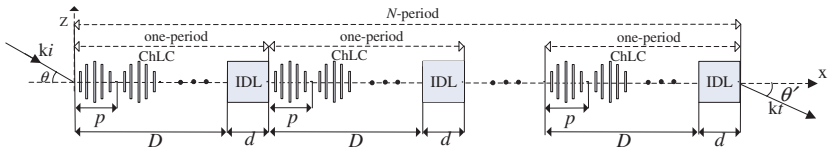

Fig. 1. Schematic drawing of ChLC-IDLs structure used in the simulations for oblique incidence, the propagation vector ***k*** lies in the *x*–*z* plane.

of IDL is *d*. The thickness ratio $\alpha = D/d$, where *D* is the thickness of ChLCs of a single pitch, which is set to $D = 0.5p$. The incident light is oblique to the surface of the ChLC-IDLs with the incident angle θ. The direction vector of the LC layer is $\hat{n} = [\cos(q_0 z), \sin(q_0 z), 0]$, and the dielectric tensor function $\varepsilon(z)$ is $\varepsilon_{ij} = \varepsilon_\perp \delta_{ij} + \Delta\varepsilon n_i n_j$, where $(i, j) \in \{x, y, z\}$, δ_{ij} is the Kronecker delta and $\Delta\varepsilon = (\varepsilon_{||} - \varepsilon_\perp)$. Only the case of $\mu = 1$ is considered, since we are interested in the visible light region.

2. Berreman Fast 4×4 matrix method

The extended Jones matrix and Berreman Fast 4×4 matrix methods have been widely used in single display cell simulations [19,20,22]. Considering that interference effect dominates in ChLC-IDLs, we use the Berreman Fast 4×4 matrix method. Numerical analysis of the optical transmission characteristics in the helical structure is performed based on the Berreman Fast 4×4 matrix, which is able to calculate light propagating within a medium with refractive index varying along one direction.

Generally, a monochromatic plane wave consists of the electric $[E(r, t)]$ component and the magnetic $[H(r, t)]$ field component, which can be written as $E(r, t) = E(r)\exp(j\omega t)$ and $H(r, t) = H(r)\exp(j\omega t)$, where ω is angular frequency of the monochromatic plane wave. The *x*–*y* components of the electric field *E* and the magnetic field *H* can be written as:

$$\begin{pmatrix} E_x \\ E_y \\ H_x \\ H_y \end{pmatrix} = \psi(z) e^{-i\omega(t - \eta x/c)} \tag{1}$$

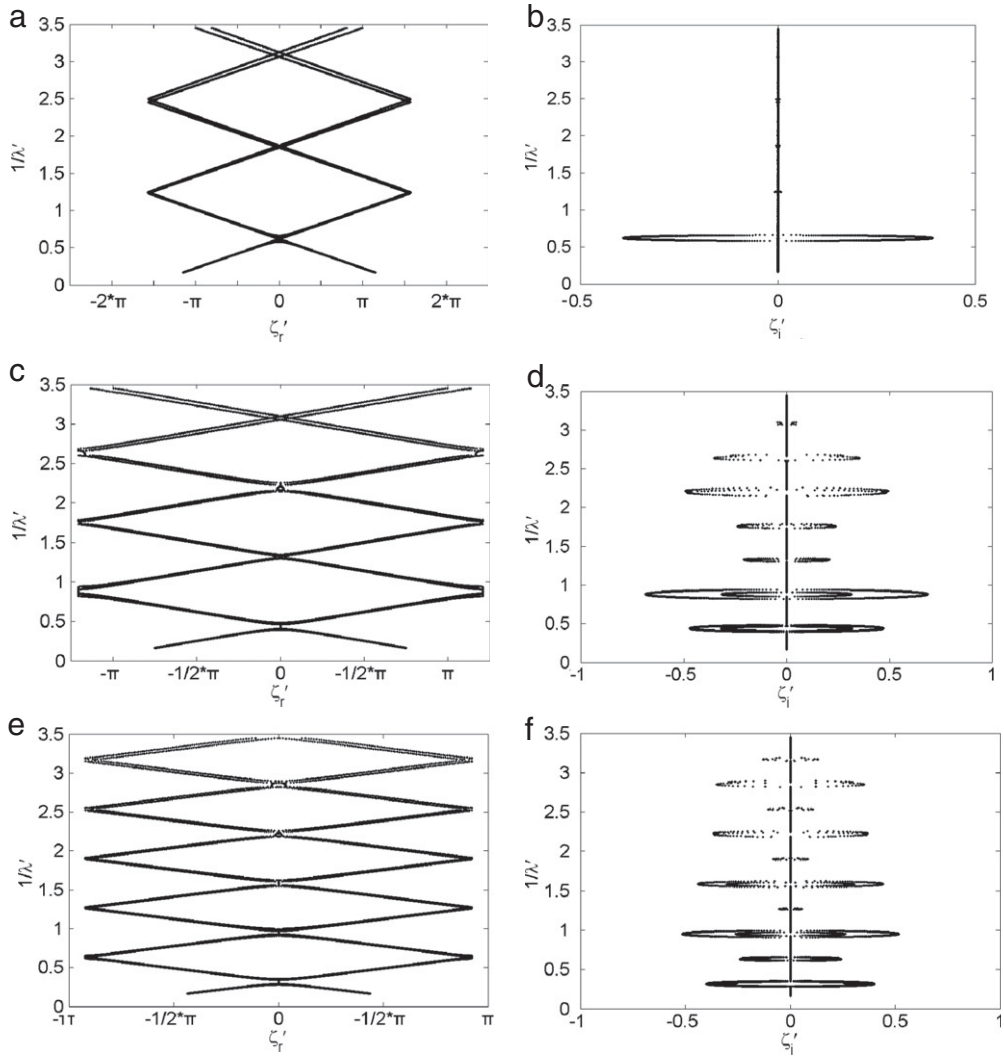

Fig. 2. Dispersion Relationship of ChLC-IDLs with different thickness of IDL (d).

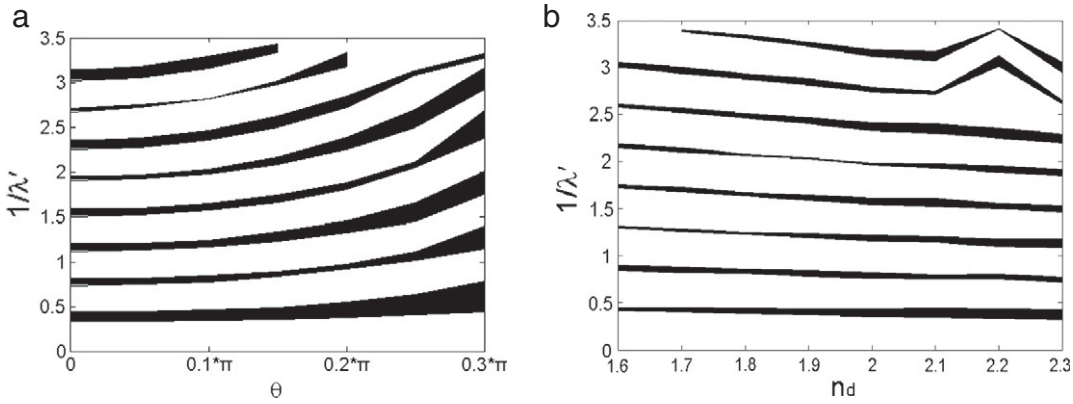

Fig. 3. (a) Evolution of the band structures with the increasing of incident angle θ, $D=0.5p$, $d=0.25p$ and $n_d=2.2$; (b) Evolution of the band structures with n_d varied from 1.6 to 2.3, $D=0.5p$, $d=0.25p$ and $\theta=0$.

In this case, the light wave is assumed to propagate in the *x*-*z* plane. The propagation function of light along the *z* axis with frequency ω is given by

$$\frac{d\psi(z)}{dz} = i\frac{\omega}{c}B(z)\psi(z) \tag{2}$$

where *B* is the Berreman 4×4 matrix. Assuming nonmagnetic medium ($\mu=\boldsymbol{I}$, $\boldsymbol{I}$: unit matrix) and a constant dielectric tensor ε, the Berreman matrix can be written as:

$$B = \begin{pmatrix} -\eta\frac{\varepsilon_{zx}}{\varepsilon_{zx}} & \eta\frac{\varepsilon}{\varepsilon_{zz}} & 0 & 1-\frac{\eta^2}{\varepsilon_{zx}} \\ 0 & 0 & -1 & 0 \\ \varepsilon_{yx}\frac{\varepsilon_{zx}}{\varepsilon_{zz}}-\varepsilon_{yx} & \eta^2-\varepsilon_{yx}+\varepsilon_{yx}\frac{\varepsilon_{zy}}{\varepsilon_{zz}} & 0 & \eta\frac{\varepsilon_{yz}}{\varepsilon_{zz}} \\ \varepsilon_{xx}-\varepsilon_{xz}\frac{\varepsilon_{zx}}{\varepsilon_{zz}} & \varepsilon_{xy}-\varepsilon_{xz}\frac{\varepsilon_{zy}}{\varepsilon_{zz}} & 0 & -\eta\frac{\varepsilon_{xz}}{\varepsilon_{zz}} \end{pmatrix} \tag{3}$$

As illustrated in Fig. 1, the entire ChLC-IDLs system is divided into *N* layers, where η is proportional to the *x* component of the wave vector *k*. If *B* is constant in interval $(z, z+h)$, the solution of Eq. (2) is

$$\psi(z+h) = P(z,h)\psi(z) \tag{4}$$

where $P(z, h)$ is the local propagation matrix related to Berrman matrix *B*. Within a period *L*, the propagation matrix $F=P_NP_{N-1}\cdots P_1$. P_n is the propagation matrix in every interval. When $B(z)$ is a periodic function of *z*, such as in a ChLC, it is convenient to calculate the propagation matrix for one period.

$$\psi(z+L) = F(z)\psi(z) \tag{6}$$

The Bloch–Floquet theorem requires that

$$\psi(z+L) = -\exp(i\zeta L)\psi(z) \tag{7}$$

In every Berreman matrix, $\eta=n_0\sin(\varphi)$, where n_0 is the refractive index of the input medium and φ is the incident angle. For a given ω and η, the optical eigenmodes are characterized byζ, which are given by the Eigen equation

$$\det|F + I\exp(i\zeta L)| = 0 \tag{8}$$

where $\boldsymbol{I}$ is the 4×4 identity matrix. In Eq. (8), ζ illustrates the phase difference between the wave function $\psi(z)$ and $\psi(z+L)$ with any *z*; hence, ζ can be determined uniquely, which means that it is independent of *z*.

3. Results and discussion (1): dispersion relation

In the numerical calculations, we do not take account of the effects of optical dispersion or absorption at first [21]. The interval *h* is chosen as $h=L/200$. For convenience, the wavelength λ is normalized by the

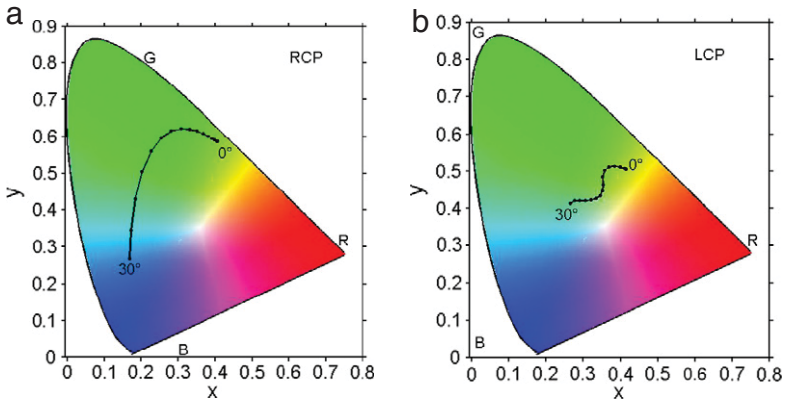

Fig. 4. Reflective light CIE-1931 chromaticity diagrams of the ChLCs without IDLs, $n_e=1.7$, $n_o=1.5$. The incident light is white light. (a) and (b) represent RCP and LCP incident light, respectively. The continuous lines represent the trajectories of the reflected light chromaticity as the incident angle increases.

helical pitch p, i.e. $\lambda' = \lambda/p$ (the visible light range is $\lambda' \in (0.45, 1)$), and hence the corresponding normalization must be made for $\zeta' = p\zeta$. The dispersion relation between ζ' and $1/\lambda'$, was calculated for different d as shown in Fig. 2.

Fig. 2 shows the relation of frequency versus the real and imaginary parts of the Bloch wave number $\boldsymbol{k}$, when $d = 0.0$ (a) and (b), $0.15p$ (c) and (d), $0.35p$ (e) and (f), respectively, where all the other parameters are kept constant. We set $D = 0.5p$, $n_d = 2.2$, and the incident degree $\theta = 0$. Fig. 2(a) and (b) show the dispersion relations of the real and imaginary parts of ζ', ζ'_r and ζ'_i which characterize the propagation along the helical axis in the first Brillouin region ($-3/2\pi \le \zeta'_r \le 3/2\pi$). The PGBs represent the first or higher order Bragg reflections in PCs. Since the imaginary part of wave number $\boldsymbol{k}$ represents the attenuation of light, the frequency ranges with the nonzero imaginary part of the Bloch wave number $\boldsymbol{k}$ represent PBGs as shown in Fig. 2 (b), (d) and (f). In Fig. 2 (b) it is shown that the width of the PBGs is infinitesimally small, except the first PBGs. Fig. 2(d) and (f) show that as d increases, the number of PBGs increases; moreover, one can see the first and second PBGs shift to the longer wavelength in the visible light region.

In Fig. 3 (a), $D = 0.5p$, $d = 0.25p$, IDL refraction index $n_d = 2.2$, the angle θ is varied from 0 to 0.3π. It is seen that the position and width of the PBGs are functions of the incident angle θ. The first and second PBGs (in the visible light region) shift to shorter wavelength and the

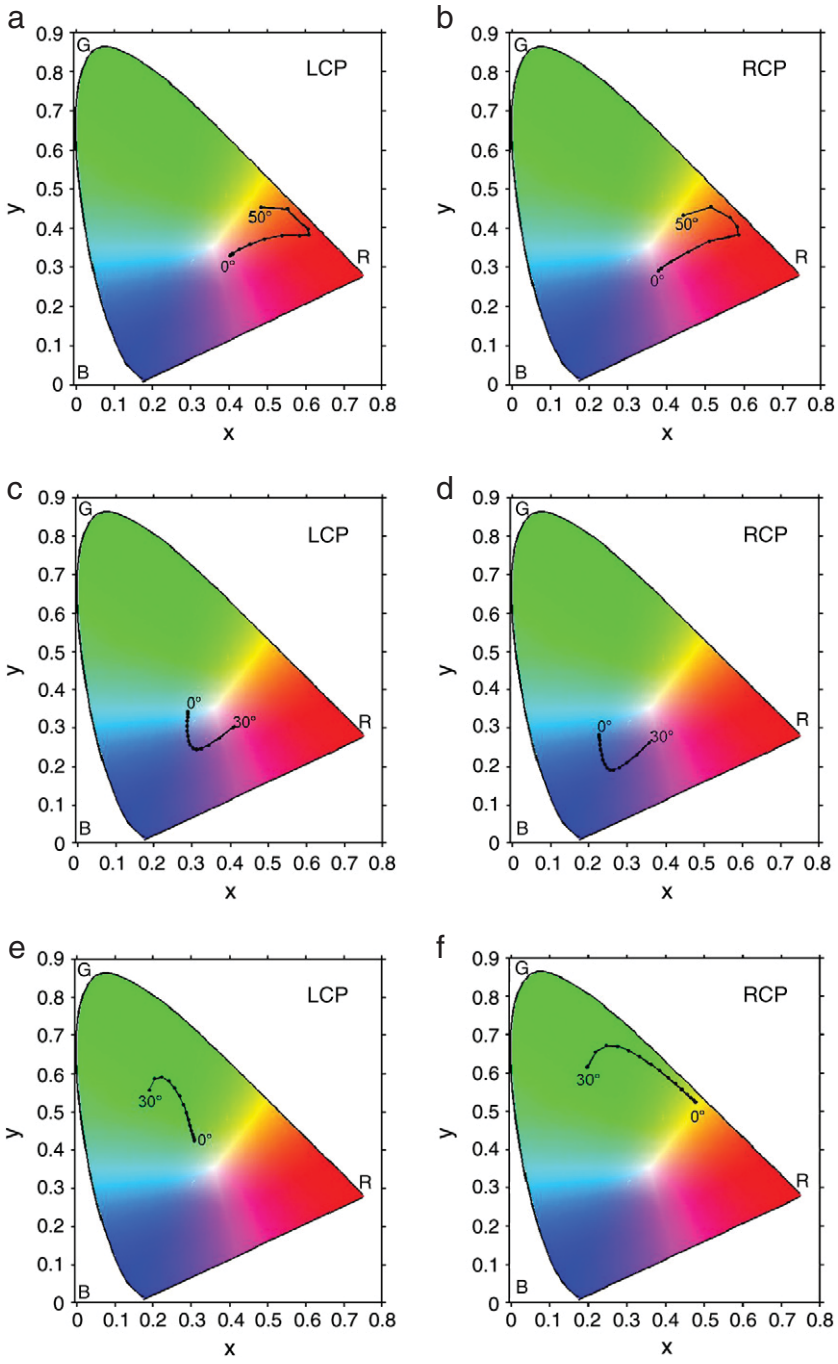

Fig. 5. Reflective light CIE-1931 chromaticity diagrams of ChLC-IDLs with different thicknesses of IDLs in the case of wavelength-independent refractive indices, (a) and (b) for $d = 0.15p$, (c) and (d) for $d = 0.25p$, (e) and (f) for $d = 0.38p$, while $n_d = 2.2$. The left and right columns represent reflective light chromaticity for RCP and LCP incident white lights respectively. The continuous lines represent the trajectories of the reflected light chromaticity as the incident angle varies from 0° to 30° or 50°.

width of the PBGs becomes wider, as θ increases. It is the same for the other band structures. In Fig. 3 (b), $D=0.5p$, $d=0.25p$, $\theta=0$. Position and width of the PBGs are the functions of n_d, and the PBGs in visible region shift to longer wavelength as n_d increases.

4. Results and discussion (2): CIE-1931 chromaticity diagram

In the study of the perception of color, one of the first mathematically defined color spaces is the CIE-1931 XYZ color space, created by the International Commission on Illumination (CIE) in 1931 [23]. The chromatic sensation of human eyes to a specific optical spectrum is usually characterized by a chromaticity diagram. Fig. 4 illustrates the CIE-1931 chromaticity diagram of the ChLCs with different incident angles of white light. Fig. 4(a) and (b) show the reflective color for right circularly polarized (RCP) and left circularly polarized (LCP) incident light, respectively. For comparison, we did numerical calculations for the system consisting of ChLCs without IDLs, which exhibits only one reflective color located in the green region. As the incident angle increases, the RCP reflective color moves towards the blue region with obvious color shift; however, the LCP reflective color moves within the green region with small color shift.

In Fig. 5, the chromaticity diagrams of ChLC-IDLs are shown with $D=0.5p$, $nd=2.2$, which are quite different from those without IDLs. In this case, both incident LCP and RCP lights have common reflection chromaticity in red, green and blue regions. Furthermore, much less color shift is observed with the increasing of incident angle. In Fig. 5 (a) and (b), the reflection chromaticity of both LCP and RCP incident lights are located in the red region with θ varying from 0°to 50°, for

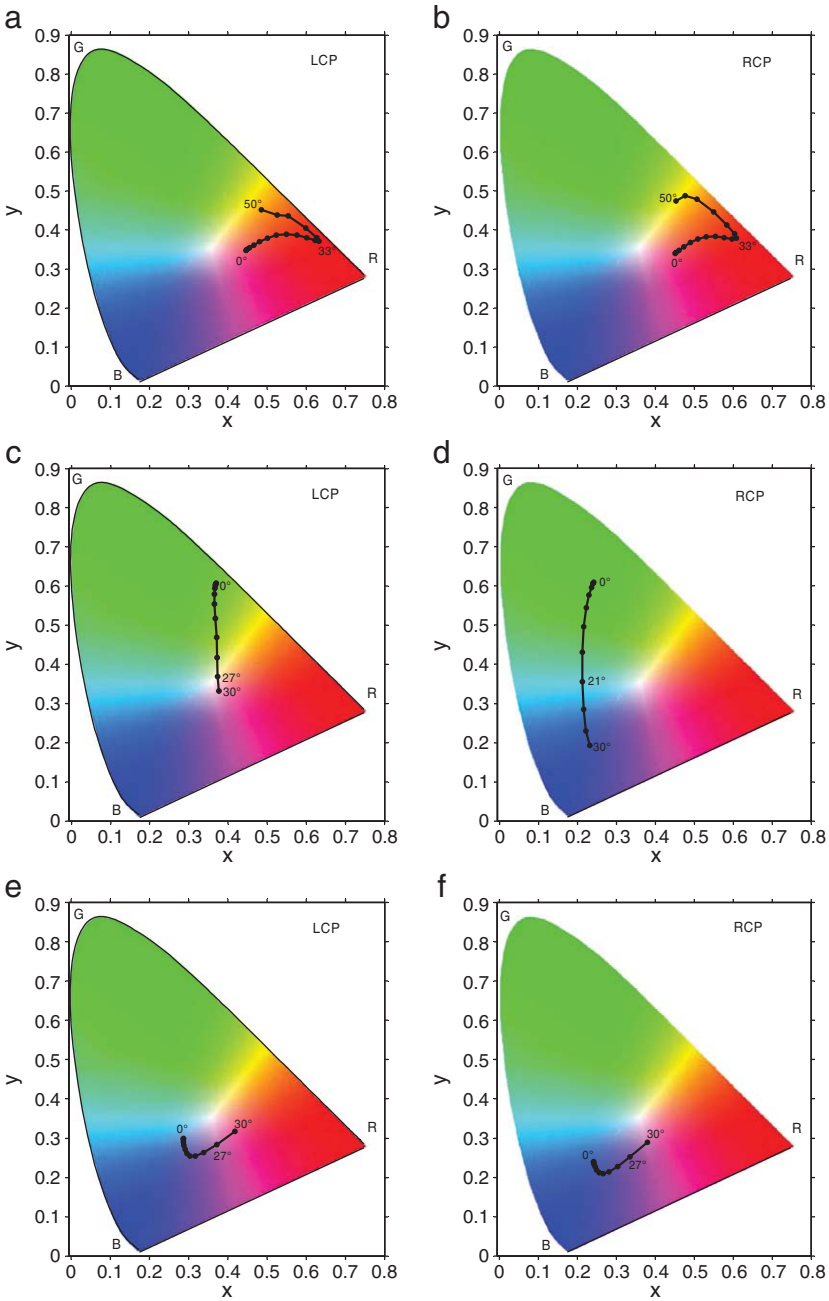

Fig. 6. Reflective light CIE-1931 chromaticity diagrams of ChLC-IDLs with different thicknesses of IDLs in the case of wavelength-dependent refractive indices, the LC material is E7 at the 20°C, (a) and (b) for $d=0.15p$, (c) and (d) for $d=0.30p$, (e) and (f) for $d=0.23p$, respectively, with $n_d=2.2$. The left and right columns represent reflective light chromaticity for LCP and RCP incident white lights, respectively. The continuous lines represent the trajectories of the reflected light chromaticity as the incident angle varies from 0° to 30° or 50°.

d = 0.15*p*; in Fig. 5(c) and (d), they are in blue region with θ varying from 0° to 30°, for d = 0.25p; while in Fig. 5(e) and (f), they are in blue region with θ varying from 0° to30°, for d = 0.38*p*. The above characteristics indicate that the proposed structures can be used as reflective color filters in liquid crystal displays to recycle energy, as they reuse the opposite circular-polarization light and increase the useful radiation by about 60% [24].

The reflective chromaticity diagrams of ChLC-IDLs are obtained when considering wavelength- dependent refractive indices in Fig. 6. Compared with the case of wavelength-independent refractive indices in Figs. 4 and 5, with the increasing of the thickness of IDLs, the reflection chromaticity can be located in different colour regions as the wavelength-independent case for LCP and RCP lights; However, in the case of the green color region, the reflective chromaticities of wavelength- dependent refractive indices are more sensitive to the incident angle. The LCs material is E7, with the data of dispersion relations at 20°C obtained from references [25,26]. In a word, one can see that the reflected light chromaticity little changes when considering the dispersion relation of refractive indices. The liquid crystals material E7 with wavelength-dependent refractive indices can be applied for ChLC-IDLs device.

5. Conclusions

We have investigated one-dimensional PCs made of ChLCs with sandwiched periodic isotropic defect layers by computing the dispersion relations based on Berreman Fast 4×4 matrix method and the reflection chromaticity diagrams of these structures. The structure exhibits two common reflection bands for both the left and right circularly polarized lights in a wide range of incident angle. Moreover, the reflection chromaticity is insensitive to the incident angle. With these features, ChLC-IDLs are expected to be employed in TFT-LCDs, in particular transflective liquid crystal displays.

Acknowledgement

This work was supported by IVO, Shanghai Jiao Tong University ChenXing Plan (Grant No. A2687B), National Natural Science Foundation of China (Grant No. 61007025, 60906039, 11004037), Shanghai Natural Science Foundation (Grant No.09ZR1414800), and Shanghai Shuguang program (Grant No.09SG13).

References

[1] E. Yablonovitch, Phys. Rev. Lett. 58 (1987) 2059.
[2] S. John, Phys. Rev. Lett. 58 (1987) 2486.
[3] G. Ma, J. Shen, Z. Zhang, Z. Hua, S.H. Tang, Opt. Express 14 (2006) 858.
[4] A.E. Miroshnichenko, E. Brasselet, Y.S. Kivshar, Appl. Phys. Lett. 92 (2008) 253306.
[5] K.L. Jim, D.Y. Wang, C.W. Leung, C.L. Choy, H.L. Chan, J. Appl. Phys. 103 (2008) 083107.
[6] H. Němec, L. Duvillaret, F. Garet, P. Kuzel, P. Xavier, J. Richard, D. Rauly, J. Appl. Phys. 96 (2004) 4072.
[7] Y.J. Xiang, X.Y. Dai, S.C. Wen, D.Y. Fan, Opt. Lett. 33 (2008) 1255.
[8] H. Taniyama, J. Appl. Phys. 91 (2002) 3511.
[9] S. Lan, K. Kanamoto, T. Yang, S. Nishikawa, Y. Sugimoto, N. Ikeda, H. Nakamura, K. Asakawa, H. Ishikawa, Phys. Rev. B 67 (2003) 115208.
[10] E.H. Boudouti, Y. Hassouani, H. Aynaou, B. Djafari-Rouhani, A. Akjouj, V.R. Velasco, J. Phys.: Condens. Matter 19 (2007) 246217.
[11] J. Schmidtke, W. Stille, Eur. Phys. J. E. 12 (2003) 553.
[12] V.I. Kopp, A.Z. Genack, Phys. Rev. Lett. 89 (2002) 033901.
[13] J. Schmidtke, W. Stille, H. Finkelmann, Phys. Rev. Lett. 90 (2003) 083902.
[14] Y.C. Yang, C.S. Kee, J.E. Kim, H.Y. Park, Phys. Rev. E 60 (1999) 6852.
[15] T. Matsui, M. Ozaki, K. Yoshino, Phys. Rev. E 69 (2004) 061715.
[16] N.Y. Ha, S.M. Jeong, S. Nishimura, H. Takezoe, Adv. Mater. 22 (2010) 1617.
[17] N.Y. Ha, Y. Ohtsuka, S.M. Jeong, S. Nishimura, G. Suzaki, Y. Takanishi, K. Ishikawa, H. Takezoe, Nat. Mater. 7 (2008) 43.
[18] E.M. Nascimento, F.M. Zanetti, M.L. Lyra, I.N. de Oliveira, Phys. Rew. E 81 (2010) 031713.
[19] D.W. Berreman, J. Opt. Soc. Am. 63 (1973) 1374.
[20] L.B. William, Modern Control Theory, 2nd Prentice-Hall, Englewood Cliffs, NJ, 1985.
[21] A. Sugita, H. Takezoe, Y. Ouchi, A. Fukuda, E. Kuze, N. Goto, Jpn. J.Appl.Phys. 21 (1982) 1543.
[22] Q. Hong, T.X. Wu, S.T. Wu, Liq. Cryst. 30 (2003) 367.
[23] H.R. Kang, Computational Color Technology, SPIE Press, Washington, D.C., 1993
[24] A. Hochbaum, Y. Jiang, W. Niu, IDW'99, Proceedings of the Sixth International Display Workshops, 1999, p. 379.
[25] J. Li, S.T. Wu, S. Brugioni, R. Meucci, S. Faetti, J. Appl. Phys. 9 (2005) 073501.
[26] J. Li, G. Baird, Y.H. Lin, H. Ren, S.T. Wu, J. Soc. Info. Display 13 (2005) 1017.